International Journal for Multiscale Computational Engineering, 2(2)173–188(2004)

Multiscale Simulation of Electroosmotic Transport Using Embedding Techniques

R. Qiao & N. R. Aluru**†*

Department of Mechanical and Industrial Engineering,
Beckman Institute for Advanced Science and Technology,
University of Illinois at Urbana-Champaign,
405 N.Matthews, Urbana, IL 61801,

ABSTRACT

An embedding multiscale simulation approach and its application to the electroosmotic transport in micro- and nanochannels is presented. The central idea in our multiscale simulation approach is that to analyze a coarse-scale problem, in which atomistic details are important in certain critical regions, one first performs atomistic simulation of a fine-scale system to obtain quantitative information of the system behavior in those critical regions, and then incorporates the quantitative information into continuum simulation of the coarse-scale system. To study the electroosmotic transport, two methods, namely, the modified Poisson-Boltzmann equation and velocity-embedding technique, are developed based on the embedding multiscale simulation approach. Comparison of the ion distribution and velocity profiles obtained from the multiscale simulation with the direct MD results shows very good agreement. Finally, the electroosmotic transport in a 30.0 μm wide slit channel is studied using the proposed methods, and the simulation results indicated that the classical continuum theory is not accurate at high-bulk concentrations.

*Graduate Student, Beckman Institute
**Associate Professor
†Address all correspondence to aluru@uiuc.edu

0731-8898/04/$20.00

1. INTRODUCTION

Electroosmotic transport is the movement of liquid relative to a stationary charged surface by an applied electric field. The driving force causing the liquid movement is the electrokinetic force acting on the ions in the electrical double layer, the thickness of which ranges from a few angstroms to tens of nanometers depending on the ionic strength of the solution. Because of its ease of control and scalability of the flow-rate at micro- and nanoscale, electroosmotic transport has attracted considerable attention in recent years [1–3]. It is now routinely used in microfluidic devices, and more recently in nanofluidic systems [3–5].

Modeling and simulation of electroosmotic transport, based on the classical Poisson-Boltzmann (PB) equation and the Navier-Stokes (NS) equations, has explained many experimental observations and guided the design of $\mu-$TAS (micro-Total-Analysis-Systems) [6–8]. The effectiveness of these simulations relies on the knowledge of the $\zeta-$potential or the electrokinetic charge density σ_{ek} on an imaginary shear plane [9] where the velocity is assumed to be zero. However, neither of these quantities (ζ or σ_{ek}) can be measured directly in the experiments, and in many cases, the value calculated from the surface-charge density and the electrolyte concentration (both can be measured directly in experiments) is not accurate as the PB and the NS simulations based on the calculated ζ or σ_{ek} deviate from experiments [10, 11]. Such a deviation is mainly caused by the fact that the continuum theory may no longer be valid very close to the channel wall [12]. For example, the ion concentration near the channel wall may be strongly influenced by the molecular ion-surface interactions and the water structure near the surface, and the fluid viscosity can be strongly influenced by the fluid layering near the surface. However, these effects, which originate mainly from the finite size of the ions and water molecules, are neglected in the classical continuum theory describing the electroosmotic transport. Therefore, to predict the electroosmotic transport with good accuracy, one needs to resolve the atomistic details of the ion distribution and velocity profile near the channel wall, and atomistic scale simulation, e.g., molecular dynamics (MD) simulation, becomes necessary. In MD simulation, the ion-ion, ion-wall, and ion-water interactions are calculated explicitly, the trajectory of the system is integrated by using classical mechanics and various measurables, e.g., ion concentration and bulk velocity, are obtained from statistical averaging. Therefore, by using proper interaction potentials between the atoms in the system, MD simulation can provide a quantitative understanding of the various physical processes involved without relying on the many assumptions made in the continuum theory. However, because of the high computational cost, MD simulations can probe only a very limited time (e.g., tens of nanoseconds) and length scale (e.g., a few nanometers). As the near-wall region, where the atomistic details are important, is only a small portion of the entire computational domain, a multiscale simulation approach can be efficient. In a multiscale approach, the near-wall region is modeled by using atomistic simulation, and the rest of the channel is modeled by using the classical continuum theory. Various multiscale simulation techniques have been developed in the past to study the fluid flow with localized atomistic characteristics [13–15]. In these techniques, the atomistic simulation and continuum simulation are performed simultaneously, and the effective interface coupling of atomistic and continuum simulations is a challenging research topic. In addition, the implementation of these techniques is usually complicated and thus cannot be used very easily. In this paper, we propose a multiscale simulation method that is based on the embedding technique. The central idea is to perform atomistic simulation of a smaller or a fine-scale system to obtain quantitative information of the flow in certain critical regions of a bigger or coarse-

scale system (e.g., the near-wall region in electroosmotic flows) and to incorporate the quantitative information into continuum simulation of the coarse-scale system. Compared to the interface coupling approaches, such a multiscale approach is computationally less demanding and is much easier to implement.

The rest of the paper is organized as follows: Section 2 describes the continuum and atomistic simulation of electroosmotic transport and compares the ion distribution and fluid velocity obtained from the two approaches. Section 3 describes the proposed embedding multiscale simulation method and presents results for electroosmotic transport in slit channels that are 6.00 nm and 30.00 μm in width using the multiscale approach. Finally, conclusions are presented in Section 4.

2. ELECTROOSMOTIC FLOW MODELING: CONTINUUM AND ATOMISTIC APPROACHES

In this paper, we focus on the study of electroosmotic transport of an electrolyte solution in straight flat channels (the channel width is in the z direction, and the flow is along the x direction, see Fig. 1) with no externally applied pressure gradient.

2.1. Continuum Simulation

For electroosmotic transport in a straight flat channel with a uniform charge density on the channel walls, the continuum mathematical description is based on the PB equation (1) and the Stokes equation (2)

$$\frac{\partial^2 \psi(z)}{\partial z^2} = -\frac{q}{\epsilon} \sum_{i=1}^{N} \tilde{z}_i c_{i,0} e^{-\tilde{z}_i q \psi(z)/k_B T} \qquad (1)$$

$$\frac{d}{dz}\left(\mu \frac{du(z)}{dz}\right) + \sum_{i=1}^{N} q \tilde{z}_i c_i(z) E_{ext} = 0, \qquad (2)$$

where $\psi(z)$ is the potential induced by the charges on the channel wall and the ions in the channel, q is the electron charge (i.e., 1.6×10^{-19} C), $\tilde{z}_i$ is the valency of the ion specie i, $c_{i,0}$ is the concentration of ion i at the reference plane (the channel center plane in our case) where ψ is zero, ϵ is the permittivity of the fluid in the channel, k_B is the Boltzmann constant, T is the temperature, $u(z)$ is the velocity of the fluid, μ is the dynamic viscosity of the fluid, $c_i(z)$ is the concentration of ion specie i across the channel, which is related to the potential ψ by $c_i = c_{i,0} e^{-\tilde{z}_i q \psi(z)/k_B T}$, and E_{ext} is the external electric field applied along the channel.

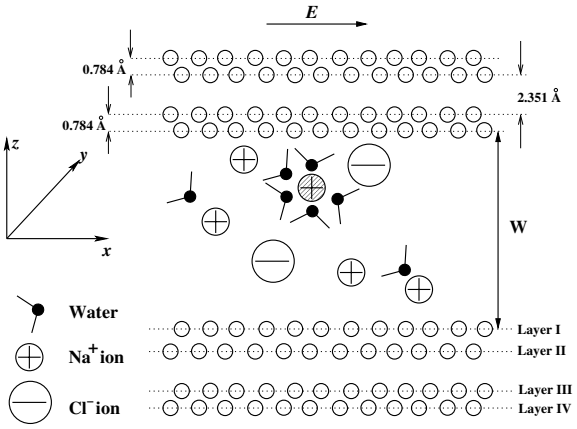

FIGURE 1. A schematic of the channel system under investigation. The two channel walls are symmetrical with respect to the channel center line. The channel width W is defined as the distance between the two innermost wall layers. For the coordinate system chosen, $z = 0$ corresponds to the central plane of the channel system.

The boundary conditions for Eqs. (1) and (2) are

$$\left.\frac{d\psi(z)}{dz}\right|_{z=\pm h/2} = \pm \frac{\sigma_s}{\epsilon} \qquad (3)$$

$$u(z)|_{z=\pm h/2} = 0, \qquad (4)$$

where $z = \pm h/2$ corresponds to the location of the lower and the upper channel wall and σ_s is the charge density on the channel walls.

Equations (1) and (2) are solved numerically in the present research. The relative permittivity of water is taken as 81, which is the re-

ported value for SPC/E water at 300 K [16, 17]. The dynamic viscosity of water is taken as 0.743 mPa·s in our continuum simulations because this gives the best match to the velocity profile in the central portion of the channel. We have simulated Poiseuille flow of pure SPC/E water at a peak strain rate of 4.7×10^{10} s^{-1}, temperature of 300 K, and the dynamic viscosity of water was determined to be 0.683 mPa·s, which is within 5% of the reported value for SPC/E water [18]. For an ionic solution, using a viscosity higher than that of pure water is in accordance with the experimental observations that the viscosity of an electrolyte solution increases as the concentration of electrolyte increases. For example, the viscosity of 0.89 M NaCl solution at 293 K is about 8.5% higher than that of pure water at 293 K [19].

2.2. Molecular Dynamics Simulation

Figure 1 shows the schematic diagram for the MD simulation of electroosmotic flow in a nanometer slit channel. Each wall is made up of four layers of silicon atoms oriented in the $< 111 >$ direction. The lateral dimension of the channel wall is 4.66 $\times$ 4.22 nm, and the channel width is varied from 3.49 nm to 6.0 nm in the simulations.

In the simulations, the outermost wall layers (i.e., layer I of the lower channel wall and its counterpart in the upper channel wall) are partially charged. Here we assume that the charges are uniformly distributed among the wall atoms. Because the spacing between the surface atoms is very small (less than 0.4 nm), the channel wall will appear to be smoothly charged for the charges in the channel system [20] and this mimics the smooth surface charge density assumed in the PB equation.

MD simulations were performed using a MD package Gromacs [21, 22]. The simulation details have been reported in a previous paper [12] and here we mention only the model employed for the molecules in the system and the calculation of the electrostatic force. The water molecules are modeled by using the SPC/E model [16], i.e., the water molecule is rigid, and the hydrogen and oxygen atoms are modeled as point charges. The SPC/E model is chosen because it can reproduce the dielectric constant and dynamic properties of water quite well compared to other water models. The ions (Na^+ and Cl^- ions) are modeled as charged Lennard-Jones atoms. Since the long-range electrostatic interactions play a vital role in determining the ion distribution in the channel, the electrostatic interactions must be computed without truncation. To compute the electrostatic interaction, we chose the Particle Mesh Ewald (PME) method [23], which involves no truncation for the long-range electrostatic interactions. The original PME technique assumes periodicity in all three directions. However, there is no periodicity in the channel width direction (z direction, see Fig. 1) in our channel system. To compute the electrostatic interactions in our system with reduced periodicity, we have (i) modified the original PME algorithm by adding a correction term [24] to the standard Ewald summation formula, and (ii) elongated the simulation box in the z direction to be three times larger than the channel width.

Starting from a random configuration, the system was simulated for 1.0 ns so that the system has reached steady state. A production run of 10–11 ns was then performed to gather the statistics of various quantities, e.g., streaming velocity. The density and velocity profile across the channel are computed by using the binning method [25]. The flow is driven by an external electric field E_{ext} applied along the channel in the x direction. Because of the extremely high thermal noise, a strong electric field was applied in our simulations so that the fluid velocity can be retrieved with reasonable accuracy. To remove the heat generated during the simulation, a Berendsen thermostat [26] with a time constant of 0.1 ps was used to maintain the fluid temperature to 300 K. Table **1** summarizes the MD simulations performed in this paper.

Table 1. Summary of the simulations performed

Case	Channel width (nm)	σ_s (C/m^2)	# Water molecules	# Ions	E_{ext} (V/nm)	Simulation time (ns)	CPU time † (hours)
1	3.49	+0.13	2094	35 Cl^-, 3 Na^+	−0.36	13.6	213.5
2	3.49	−0.13	2124	3 Cl^-, 35 Na^+	0.25	13.6	213.5
3	6.00	+0.13	3629	38 Cl^-, 6 Na^+	−0.36	12.0	329.5
4	6.00	−0.13	3629	6 Cl^-, 38 Na^+	0.25	12.0	329.5

† Simulations were performed on a 2.4 GHz Platinum machine with 1.0 GB memory.

2.3. Comparison of Continuum and MD Simulation Results

2.3.1. Ion Distribution

Figure 2 shows the concentration profiles of Na^+ and Cl^- ions across the channel for case 1, where the channel width is 3.49 nm and the wall charge density is +0.13 C/m^2. The prediction of ion distribution from the PB equation is also shown for comparison. In solving the PB equation, we set the closest approach of Na^+ and Cl^- ion toward the channel wall to be 0.44 nm and 0.35 nm, respectively. To solve the PB equation, one also needs the bulk concentration of the electrolyte solution, i.e., the ion concentration of the bath that is in equilibrium with the electrolyte solution in the channel. Since the MD simulation is performed in a NVT ensemble [25], such a bulk concentration does not appear explicitly in the MD simulation. To compute the bulk concentration, we note that at thermal equilibrium, the concentrations of Na^+ and Cl^- ions at the channel center are given by

$$c_{Na^+}(z=0) = c_{bulk}\, e^{-q\psi/k_BT} \tag{5}$$

$$c_{Cl^-}(z=0) = c_{bulk}\, e^{q\psi/k_BT}, \tag{6}$$

where c_{bulk} is the bulk concentration of Na^+ and Cl^- ions, and ψ is the electric potential at the channel center. Combining Eqs. (5) and (6), the bulk concentration of electrolyte solution can be computed by

$$c_{bulk} = \sqrt{c_{Na^+}(z=0)\, c_{Cl^-}(z=0)}. \tag{7}$$

MD results for a 3.49 nm wide channel indicate that the Na^+ and Cl^- ion concentration at the channel center are 0.122 M and 0.263 M, respectively. Therefore, using Eq. (7), the bulk concentration of the electrolyte is determined as 0.179 M. Figure 2 shows that, near the channel wall, the counter-ion concentration from MD simulation is much higher compared to the PB prediction, while in the central portion of the channel, the PB prediction is higher compared to the MD results. This is similar to what was reported in our previous work [12], and the reason for the deviation is that the classical PB equation fails to account for the molecular interactions between the counter-ion and the channel wall. Since the surface charges are screened much more significantly by the counter-ions near the channel wall in the MD simulation compared to that predicted by the PB equation, the counter-ion concentration in the central portion of the channel is lower than what is predicted by the PB equation. This also causes the co-ion concentration in the central portion of the channel to be higher compared to what is predicted by the PB equation.

Figure 3 shows the concentration profiles of

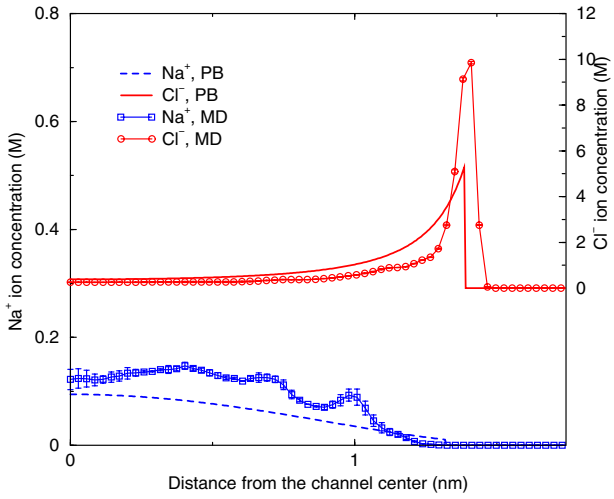

FIGURE 2. Na^+ and Cl^- ion concentrations across the channel for case 1 (W = 3.49 nm, $\sigma_s = +0.13$ C/m^2). The error bars are estimated from three continuous MD runs each of 4.2 ns long.

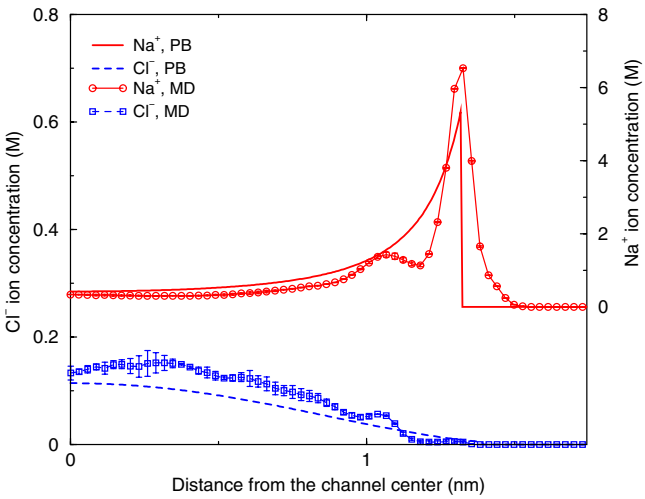

FIGURE 3. Na^+ and Cl^- ion concentrations across the channel for case 2 (W = 3.49 nm, $\sigma_s = -0.130$ C/m^2). The error bars are estimated from three continuous MD runs each of 4.2 ns long.

Na^+ and Cl^- ions across the channel for case 2, where the channel width is 3.49 nm and the wall charge density is -0.13 C/m^2. The observations are similar to that of the case 1 except that there is a much more distinct second concentration peak near the channel wall for the counter-ion. As explained in a previous paper, this is mainly caused by the interactions between the counter-ion and its nearby water molecules [12].

2.3.2. Velocity Profile

Figure 4 shows the velocity profile across the channel for case 1. The velocity profile obtained from the continuum flow theory, substituting the ion concentration calculated by obtained from the MD simulation into Eq. (2) and using the boundary condition specified in Eq. (4), is also shown for comparison. We observe that the continuum flow theory prediction using a constant viscosity of 0.743 mPa·s overestimates the velocity in the entire channel. This is because the continuum calculation fails to take into account the fact that the viscosity near the channel wall is much higher compared to its bulk value. As has been reported in [27], the viscosity of water increases dramatically in the near-wall region where the ion concentration is high. Such a dramatic increase of viscosity seems to be related to the high electric field strength [9], layering of fluid molecules [10], and the high concentration of ions near the channel wall. However, a comprehensive theory accounting for all the effects is not yet available.

The question of whether the continuum flow theory based on a constant viscosity can predict the flow behavior in the central part of the channel is an interesting one. We observe that, if the predicted velocity is shifted down by about 10.7 m/s, the continuum prediction matches the MD velocity at a distance δ away from the channel wall, i.e., the continuum prediction matches the MD simulation result very well in the central portion of the channel. This is equivalent to saying that if the velocity at a position δ away from the channel wall is given

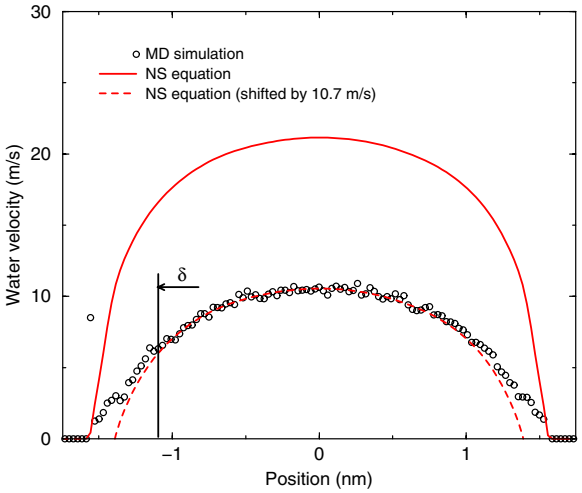

FIGURE 4. Comparison of water velocity profile across the channel for case 1 (W = 3.49 nm, $\sigma_s = +0.13$ C/m^2) as predicted by the MD simulation and by the continuum flow theory.

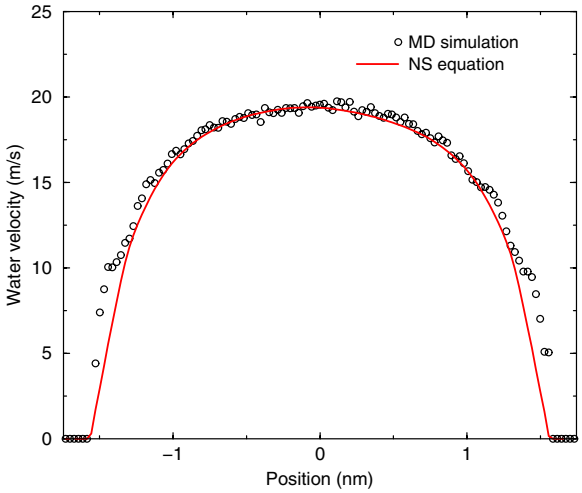

FIGURE 5. Comparison of water velocity profile across the channel for case 2 (W = 3.49 nm, $\sigma_s = -0.130$ C/m^2) as predicted by the MD simulation and by the continuum flow theory.

as the boundary condition to the Stokes equation (2), then the continuum flow theory based on a constant viscosity can still be used to predict the velocity in the central part of the channel. Figure 4 also indicates that the nonslip boundary condition is applicable to the case studied. However, the nonslip plane is not located at the center of mass of the innermost layer of the channel walls (i.e., layer I in Fig. 1), but is located at approximately 0.16 nm from the channel wall where the water concentration is almost zero.

Figure 5 shows the velocity profile across the channel for case 2. We observe that though the NS equation prediction deviates from the MD result near the channel wall, it agrees quite well with the MD result in the central portion of the channel. Comparison with the results for case 1 (see Fig. 4) indicated that the viscosity variation of water near the channel wall is not significant. This suggests that the viscosity of water near the channel wall also depends on the sign of the surface charge or the counter-ion type, which cannot be predicted by the continuum theory. However, the exact mechanism for such a dependence is not clear at present.

In summary, it is clear that though the PB and the NS equations can predict the ion distribution and velocity profiles in the channel qualitatively, they fail to predict the ion distribution and velocity profile near the channel wall accurately. This is mainly caused by the fact that (i) ions and water molecules are finite in size and the molecular interactions between them become factors influencing the ion distribution as the ions approach the channel wall, and (ii) the water structure (e.g., density and water dipole orientation) near the channel wall is significantly different from that in the bulk, and this can influence the ion distribution and velocity profiles significantly.

3. MULTISCALE SIMULATION BASED ON EMBEDDING TECHNIQUES

From Section 2, we observe that near the channel wall, various atomistic characteristics (e.g., finite size of the ions, layering of water molecules) that were neglected in the clas-

sical continuum theory for the electroosmotic flow become important. In order to predict the electroosmotic flow in the entire channel accurately, one has to capture these atomistic details in the near-wall region. Multiscale simulation can be very helpful in such a scenario. In this paper, we propose a multiscale simulation method that is based on the embedding technique. Figure 6 shows the schematics of the embedding technique. The central ideas in the embedding technique are

1. To simulate a wider (or coarser) length-scale problem (see Fig. 6a), we first set up an axillary smaller (or finer) length scale problem (see Fig. 6b) using similar input conditions (e.g., wall surface charge density) such that the near-wall noncontinuum behavior is captured.

2. A MD simulation is performed on the finer length-scale problem.

3. The MD results from the finer scale channel are embedded into the continuum simulation of the coarser length-scale problem.

For this approach to be accurate, the size of the fine-scale problem must be large enough such that all the critical regions in the coarser length-scale problem, where atomistic details are important, are included in the auxiliary problem. For this approach to be efficient, the size of the fine-scale problem must be much smaller compared to the size of the original system, i.e., $W_1 \ll W_0$. In practice, the size of the auxiliary problem is chosen as a compromise between these two objectives.

In the rest of this section, we describe the two embedding methods that we have developed to compute the ion concentration and velocity distribution in an electroosmotic flow.

3.1. Modified Poisson-Boltzmann Equation

In Section 2.3.1 we have shown that the molecular wall-ion, water-ion, and ion-ion interactions

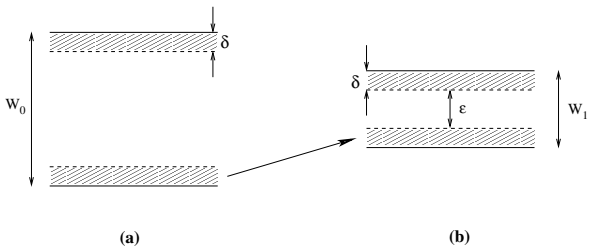

FIGURE 6. Schematics of the embedding technique for multiscale simulation. **(a)** represents the original coarser length-scale problem and **(b)** represents auxiliary fine-scale problem set up to solve the coarser length-scale problem. W_0 and W_1 are the characteristic length scales of the two systems. The shaded areas of width δ denote the critical regions where atomistic details are important in determining the system behavior. The region of width ϵ in panel **(b)** is a buffer region.

are important factors influencing the ion distribution in the channel. The classical Poisson-Boltzmann equation considers these interactions only in a mean-field fashion and fails to account for the molecular nature of the ion, water, and the wall (e.g., water is modeled as a continuum with a constant permittivity). In this section, we propose a modified Poisson-Boltzmann equation that takes into account the wall-ion, water-ion, and ion-ion interactions in a lumped manner.

Here we employ the concept of electrochemical potential correction to account for the interactions neglected in the classical Poisson-Boltzmann equation. At thermodynamic equilibrium, the electrochemical potential of an ion should be constant in the entire system, i.e.,

$$\mu_i = \tilde{z}_i q\psi + k_B T\, log c_i + \phi_{ex,i} = k_B T\, log c_{0,i}, \quad (8)$$

where $\tilde{z}_i$ is the valency of ion i, ψ is the electric potential in the system, c_i is the ion concentration, $\phi_{ex,i}$ is the electrochemical potential correction of ion i, and $c_{0,i}$ is the concentration of ion i when the electric potential and the electrochemical potential correction term are zero. Based on Eq. (8), the ion concentration can be

expressed as

$$c_i = c_{0,i}\, e^{-\frac{\tilde{z}_i q\psi}{k_B T}} e^{-\frac{\phi_{ex,i}}{k_B T}}. \tag{9}$$

Substituting Eq. (9) into the Poisson equation (10), we have

$$\nabla^2\psi = -\frac{q}{\epsilon}\sum_{i=1}^{N}\tilde{z}_i c_i, \tag{10}$$

$$\nabla^2\psi = -\frac{q}{\epsilon}\sum_{i=1}^{N}\tilde{z}_i c_{0,i}\, e^{-\frac{\tilde{z}_i q\psi}{k_B T}} e^{-\frac{\phi_{ex,i}}{k_B T}}, \tag{11}$$

where N is the total number of ionic species and is equal to 2 in all our simulations.

The electrochemical potential correction term accounts for the deviation of the ion-water and ion-wall molecular interactions from their values at the channel center. Since the wall-ion interaction via the Lennard-Jones potential is short-ranged, and the water-ion interaction would not deviate significantly in the entire system except at positions very close to the channel wall where the water concentration is not constant, the electrochemical potential correction term is nonzero only at positions close to the channel wall.

In principle, one can calculate $\phi_{ex,i}$ provided the wall-ion, water-ion, and ion-ion interactions can be computed explicitly. However, such a calculation, if possible, is very difficult. For example, to account for the molecular nature of water, the charge-dipole interaction between water and the ion as well as other molecular interactions (e.g., the van der Waals interaction as included in the Lennard-Jones potential) will need to be considered explicitly. Here we extract the electrochemical potential correction term from the ion concentration profile obtained from MD simulation of a smaller width channel using Eq. (9). Once the electrochemical potential correction term is obtained, one can use it in the modified Poisson-Boltzmann equation (11) to simulate the ion distribution in a bigger channel with the same wall structure and similar surface charge density. In such an approach, one circumvents the difficulty of obtaining a closed form expression for the electrochemical potential correction term by utilizing the MD simulation results.

The accuracy of this approach depends on how the fine-scale problem is set up and on how significantly the electrochemical potential correction term differs in the two problems. In setting up the fine-scale problem, one needs to include the near-wall region, where the electrochemical potential correction is nonzero because of the ion-wall interactions and the localized ion-water interactions are different from that in the bulk. In this paper, we choose the width of the "near-wall region" (i.e., δ in Fig. 6) to be 1.3 nm. This is because at a position farther away from the channel wall, the molecular ion-wall interactions are negligible and localized ion-water interactions will not change appreciably as the water density oscillation is negligible. By setting up the fine-scale problem using similar operating conditions (e.g., wall charge density, wall structure, and bulk concentration) as in the original system, the electrochemical potential correction term will not differ significantly in the two problems. This is because: (i) the wall-ion interaction included in the electrochemical potential correction term is the Lennard-Jones potential, which depends only on the wall structure and the Lennard-Jones parameters and thus will not change when the channel width is increased; (ii) the water-ion interactions depend primarily on the water concentration (i.e., how closely the water molecules are packed). MD simulation results of the water concentration profile in channels of different width, but with the same surface charge density, indicate that the water concentration profile near the channel wall is independent of the channel width. In summary, the electrochemical potential correction term is primarily due to the wall effects (e.g., ion-wall interactions and wall-induced water layering). As these interactions are short-

ranged, further addition of water layers in the bulk (corresponding to a wider channel) would not affect the electrochemical potential correction term significantly. Hence, the use of the same electrochemical potential correction term for wider channels can produce reasonably accurate results.

The efficiency of this approach depends on whether the length scale of the fine-scale problem can be significantly smaller compared to the original problem. This can be achieved by choosing a small ϵ in Fig. 6. However, if the ϵ is too small in the fine-scale problem, the system behavior in one critical region may be influenced by the system behavior in another critical region (e.g., the ion distribution near the upper channel may be influenced by that near the lower channel wall), which may not exist in the original coarse-scale problem.

3.2. Velocity Embedding Technique

The results in Section 2.3.2 indicate that the continuum flow can be used to describe flow in channels as narrow as 3.49 nm, provided that viscosity variation near the channel wall is taken into account. It is, however, very difficult to obtain a closed-form expression for viscosity variation near the channel wall. To simulate electroosmotic flow in wide channels, where MD simulation can be very expensive, one possible way is to first do a MD simulation in a smaller channel under similar conditions (e.g., using the same wall structure and charge density as a wider channel) and then extract the viscosity from the MD simulation data. The extracted viscosity can then be used in continuum theory to model flow in a wider channel. In this approach, one assumes that the viscosity near the channel wall would not change appreciably when the channel width increases. This assumption typically holds since viscosity depends on the fluid properties and ion concentrations near the channel wall, and these parameters would not change significantly when the channel width changes provided that other operating conditions (e.g., wall structure and wall charge density) do not change significantly or remain the same. The evaluation of viscosity from molecular dynamics data can be difficult as one needs to compute the derivative of the velocity obtained from MD simulation. Since the velocity obtained from the MD simulation is usually very noisy, unless the simulation is carried out for a very long time, the derivative of the velocity would be even noisier leading to significant noise in the extracted viscosity. It is possible to smooth the velocity data using a filter, but this may introduce additional errors into the viscosity estimation. An alternative approach is to embed the velocity near the wall, obtained for the smaller channel, into the continuum modeling of flow in a larger channel. This approach is described below.

Figure 7 presents details on the simulation of electroosmotic flow in a large channel using velocity data obtained from MD simulation

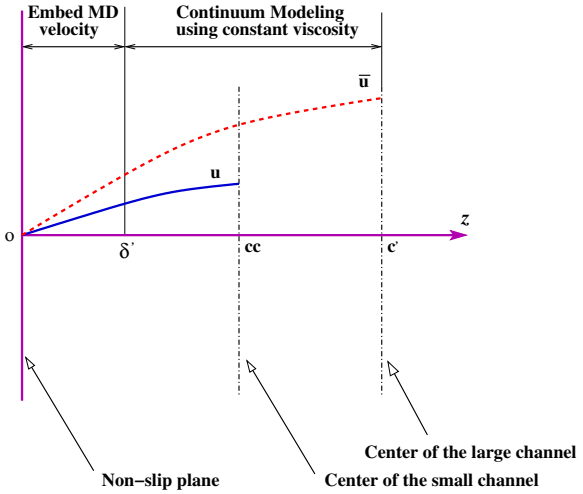

FIGURE 7. Details on the simulation of electroosmotic flow in a large channel by partitioning the channel into two regions — a near-wall region and a channel-center region. The velocity near the wall is computed by embedding the velocity obtained from MD simulation of electroosmotic flow in a smaller channel. The velocity in the channel-center region is computed by using the continuum flow theory based on a constant viscosity.

of electroosmotic flow in a small channel. For any position within δ' from the noslip plane, the velocity in the large channel is obtained by embedding the MD velocity obtained for the electroosmotic flow in a small channel. Once the velocity at $z = \delta'$ is obtained, it is used as the boundary condition for the continuum flow modeling in the central portion of the large channel using a constant viscosity. To embed the small-channel MD velocity data u within δ' from the nonslip plane of a large channel, we first integrate the momentum equation (2) from the channel centers (cc is the center of small channel and c' is the center of the large channel) to position z

$$\mu \left.\frac{du}{dz}\right|_{s=cc}^{z} = \int_{cc}^{z} -\sum_{i=1}^{N} \tilde{z}_i q c_i(s) E_{ext}\, ds \qquad (12)$$

$$\mu \left.\frac{d\bar{u}}{dz}\right|_{s=c'}^{z} = \int_{c'}^{z} -\sum_{i=1}^{N} \tilde{z}_i q \bar{c}_i(s) \bar{E}_{ext}\, ds \qquad (13)$$

where u, c, and E_{ext} are the velocity, the ion concentration, and the external electric field at a position z in the small channel, respectively. $\bar{u}$, $\bar{c}$, and $\bar{E}_{ext}$ are the velocity, the ion concentration, and the external electric field at a position z in the big channel, respectively. Using the symmetry of the velocity profile with respect to the channel center

$$\left.\frac{du}{dz}\right|_{s=cc} = \left.\frac{d\bar{u}}{dz}\right|_{s=c'} = 0 \qquad (14)$$

and dividing Eq. (13) by Eq. (12) and applying Eq. (14) gives

$$\left.\frac{d\bar{u}}{dz}\right|_z = \frac{\int_{c'}^{z} -\sum_{i=1}^{N} \tilde{z}_i q \bar{c}_i(s) \bar{E}_{ext}\, ds}{\int_{cc}^{z} -\sum_{i=1}^{N} \tilde{z}_i q c_i(s) E_{ext}\, ds} \left.\frac{du}{dz}\right|_z = F(z) \left.\frac{du}{dz}\right|_z \qquad (15)$$

where $F(z)$ is defined by

$$F(z) = \frac{\int_{c'}^{z} -\sum_{i=1}^{N} \tilde{z}_i q \bar{c}_i(s) \bar{E}_{ext}\, ds}{\int_{cc}^{z} -\sum_{i=1}^{N} \tilde{z}_i q c_i(s) E_{ext}\, ds}. \qquad (16)$$

Integrating Eq. (15) from the nonslip plane (i.e., $z = 0$) to a position z, and using the fact that the velocity is zero at the nonslip plane, we obtain

$$\bar{u}(z) = \int_{s=0}^{z} F(s) \frac{du}{ds}\, ds = = F(z)u(z) - \int_0^z \frac{dF(s)}{ds} u(s)\, ds. \qquad (17)$$

Equation (17) can be used to compute the velocity near the channel wall in large channels. Note that no derivatives of the MD velocity in the small channel are needed. Instead, one needs to calculate the derivative of the function $F(z)$. $F(z)$ is obtained by integrating the ion concentration, and it is much easier to obtain good statistics for ion concentrations in MD simulations. In principle, Eq. (17) can be applied in the region from nonslip plane to the center of the small channel (i.e., point cc in Fig. 7). However, Eq. (17) is used only in the region within δ' from the channel wall. There are two reasons for this. First, evaluation of the function $F(z)$ is difficult as we approach the center of the small channel because the integration term in the denominator is close to zero. Second, because the viscosity variation is important only near the channel wall, we can use a constant viscosity from location δ' away from the nonslip plane instead of embedding the MD velocity. In our simulations, δ' is taken to be 0.64 nm because MD simulations indicate that the viscosity variation beyond this length scale is small. As mentioned earlier, the nonslip plane is typically located at 0.16 nm from the channel wall. Hence, the region in which the velocity is obtained from embedding the MD velocity is $\delta = 0.80$ nm from the channel wall for the larger channel.

3.3. Validation of the Embedding Techniques

To test the validity of the methods described in Sec. 3.1 and 3.2, we use these methods to

calculate the ion distribution and velocity profiles in two 6.00 nm wide channels with a surface charge density of $+0.13$ C/m^2 and -0.13 C/m^2, respectively. The bulk concentrations of the electrolyte solution in the two cases are 0.19 M and 0.22 M, respectively. We use the systems in case 1 and 2 as the auxiliary fine-scale problems with a δ (see Fig. 6) of 1.3 nm and an ϵ of 0.89 nm.

Figure 8 shows the electrochemical potential correction term ϕ_{ex} calculated using the ion concentration shown in Fig. 2 and Eq. (9). Note that $\phi_{ex,i}$ is close to zero at a position of about 0.9 nm away from the channel wall. The negative ϕ_{ex} for Cl^- ion in the region $z < 1.0$ nm is mainly caused by the molecular ion-wall interactions. Note that ϕ_{ex} is positive in the region $z > 0.6$ nm for the Na^+ ion. This is mainly caused by the hydration effect. When a Na^+ ion moves toward the channel wall, it experiences a nonzero force normal to the channel wall due to its interaction with the hydration water molecules that are distributed asymmetrically around it. Such an effect is not considered in the formulation of the classical PB equation. Because of the strong attractive electrostatic interactions between Na^+−water, such a force typically pulls the Na^+ ions away from the channel wall, thus leading to a positive electrochemical potential correction term. Figure 9 shows a comparison of the Na^+ and Cl^- ion concentrations across the 6.0 nm channel with a surface charge density of $+0.13$ C/m^2 (case 3) obtained by using the modified PB equation and the electrochemical potential correction term (shown in Fig. 8) and with the MD simulation results. We observe that the modified PB equation predicts the Cl^- ion concentration in the channel quite well. The agreement of the Na^+ ion concentration is also reasonably good considering the large statistical error in the MD simulation results. Note that the statistical error of the co-ion concentration is much larger compared to that of the counter-ion, and this is because we have much less number of co-ions in the system compared to that of the counter-ions.

Figure 10 shows the electrochemical potential correction term ϕ_{ex} calculated using the ion concentration shown in Fig. 3 and Eq. (9).

Figure 11 shows a comparison of the Na^+

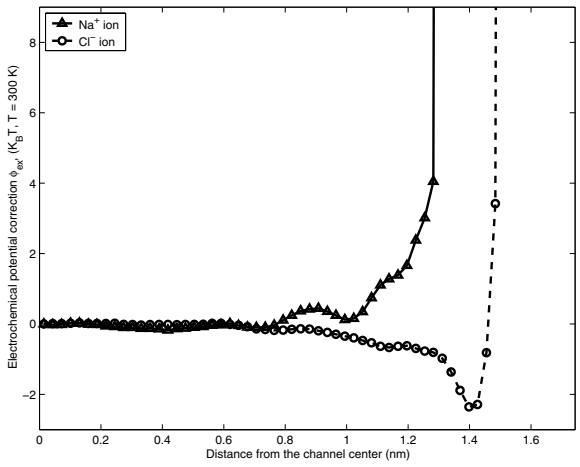

FIGURE 8. Electrochemical potential correction term for the Na^+ and Cl^- ions extracted from the ion distribution in case 1 (see Fig. 2).

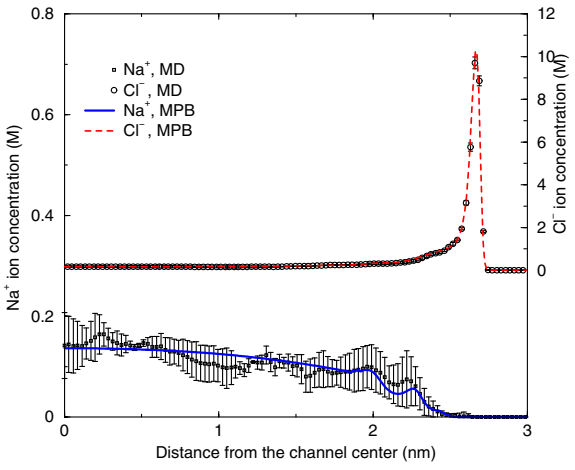

FIGURE 9. Comparison of ion concentration for case 3 (W = 6.00 nm, σ_s = $+0.13$ C/m^2) using Eq. (11) and the electrochemical potential correction term shown in Fig. 8.

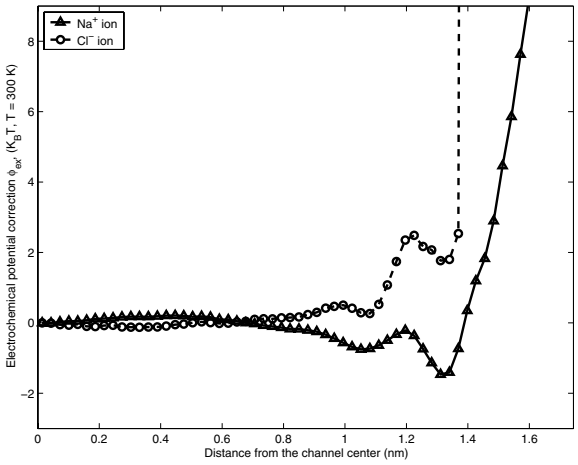

FIGURE 10. Electrochemical potential correction term for the Na^+ and Cl^- ions extracted from the ion distribution in case 2 (see Fig. 3).

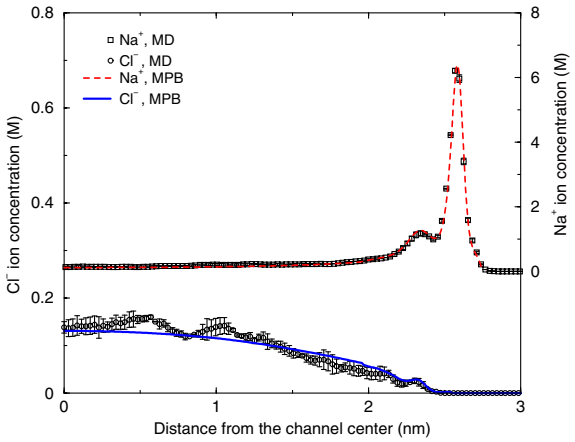

FIGURE 11. Comparison of ion concentration for case 4 (W = 6.00 nm, σ_s = −0.13 C/m^2) using Eq. (11) and the electrochemical potential correction term shown in Fig. 10.

and Cl^- ion concentrations across the 6.0 nm channel with a surface charge density of −0.13 C/m^2 (case 4) obtained by using the modified PB equation and the electrochemical potential correction term (shown in Fig. 10) and with the MD simulation results. Again, a good agreement between the multiscale simulation results and the MD results are observed.

Figure 12 shows the velocity profile for case 3 (W = 6.00 nm, σ = +0.13 C/m^2) obtained using the velocity embedding technique. The velocity in region within δ from the channel wall is embedded from the MD velocity in the same region of case 1 (W = 3.49 nm) using Eq. (17). The velocity in the central portion of the channel is computed by using a constant viscosity of 0.743 mPa·s. We observe that the velocity obtained by using Eq. (17) matches the MD simulation results quite well.

Figure 13 shows the comparison of the velocity profile for case 4 (W = 6.00 nm, σ = −0.13 C/m^2) obtained using the velocity embedding technique and MD simulation. A good agreement between the MD simulation and multiscale simulation results is again observed.

3.4. Application to Microfluidic Systems

In this section, we use the multiscale simulation method developed in this paper to investigate the electroosmotic flow inside a 30.0 μm wide channel with a surface charge density of +0.13 C/m^2 at various bulk concentrations. An external electric field of -1.0 $\times 10^5$ V/m is used to drive the flow. Using the same procedure as discussed in the previous section, we compute the ion distribution and velocity profile in the channel. Figure 14a shows the average velocity (left $y$axis) and the $\zeta-$potential (right y axis) on the channel wall obtained by using the multiscale simulation and classical continuum theory. The $\zeta-$potential is computed by using

$$\zeta = \frac{\mu u_p}{\epsilon E_{ext}} \tag{18}$$

where u_p is the maximum velocity in the channel. We observe that the electroosmotic velocity (or surface $\zeta-$potential) obtained from the continuum theory is much higher compared to the multiscale prediction. This indicates that the various effects neglected in the classical continuum theory plays an important role in determining the electroosmotic flow not only in the

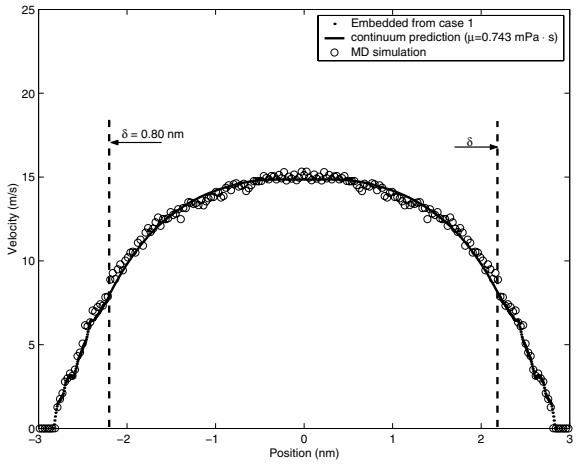

FIGURE 12. Velocity profile across the channel for case 3 (W = 6.00 nm, $\sigma = +0.13$ C/m^2). The velocity in the region within δ from the channel wall is embedded from the MD velocity in the same region of case 1 (W = 3.49 nm, $\sigma = +0.13$ C/m^2) using Eq. (17). The velocity in the central portion of the channel is computed using a constant viscosity of 0.743 mPa·s.

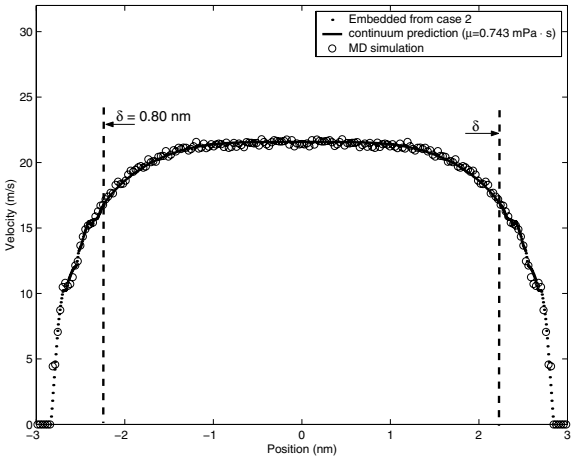

FIGURE 13. Velocity profile across the channel for case 4 (W = 6.00 nm, $\sigma = -0.13$ C/m^2). The velocity in region within δ from the channel wall is embedded from the MD velocity in the same region of case 2 (W = 3.49 nm, $\sigma = -0.13$ C/m^2) using Eq. (17). The velocity in the central portion of the channel is computed using a constant viscosity of 0.743 mPa·s.

nanochannel, but also in microchannels. This is because the driving force for an electroosmotic flow exists only within the thin electrical double layer (a few angstroms to tens of nanometers in width) near the channel wall, and since the continuum theory can not capture the ion distribution and flow behavior near the channel wall accurately, the continuum theory will not be able to predict the electroosmotic flow accurately no matter how wide the channel is. Figure 14b shows the variation of the ratio of $\zeta-$potential predicted by the multiscale simulation and classical continuum theory as a function of the bulk concentration. We observe that as the bulk concentration decreases, the difference between the prediction from continnum theory and the multiscale simulation decreases. This is because as the bulk concentration decreases, the electrical double layer, whose width is typically measured by the Debye length, extends further from the channel wall and the electroosmotic flow is less influenced by the various effects (e.g., molecular ion-wall interaction) that are neglected in the continuum theory. As a result, the accuracy of the velocity predicted by using the continuum theory improves as the bulk concentration decreases.

4. CONCLUSIONS

In this paper, we have presented embedding multiscale simulation techniques for analysis of electroosmotic flow. Specifically, a modified PB equation is used to compute the ion distribution in the channel and a velocity embedding technique is used to compute the velocity profile near the channel wall. In both methods, for a given coarse-scale problem, a molecular dynamics simulation is performed on a fine-scale problem (the fine-scale problem is similar to the coarse-scale problem except for the length scale) to obtain the ion distribution and velocity profile variation in the fine-scale problem. In the modified PB equation approach, an electrochemical potential correction term, which accounts for the various effects neglected in the

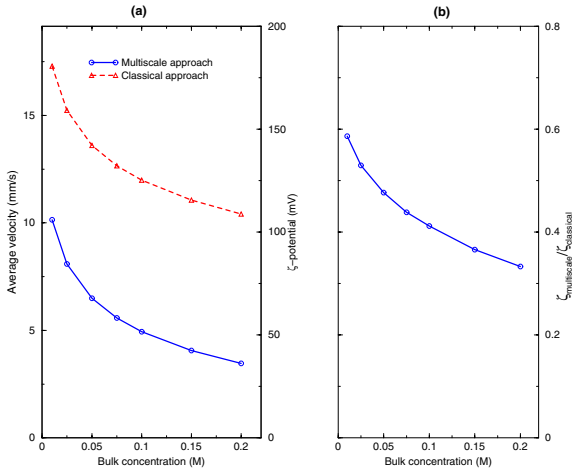

FIGURE 14. (a) Comparison of the average velocity (left axis) and $\zeta-$potential (right axis) in the 30.0 μm channel (σ = $+$0.13 C/m^2, E_{ext} = -1.0$\times$10^5 V/m) as obtained from the multiscale simulation method described in Sec. 3 and by the classical continuum theory. **(b)** Variation of the ratio of $\zeta-$potential predicted by the multiscale simulation and the classical continuum theory as a function of the bulk concentration.

classical PB equation, is extracted from the ion distribution in the fine-scale problem and used in the modified PB equation to compute the ion distribution in the original or coarse-scale problem. In the velocity embedding technique, the velocity for the coarse-scale problem in the region very close to the channel wall, where the continuum flow theory based on a constant viscosity fails, is computed by embedding the MD velocity in the same region from the fine-scale problem. The velocity profile in the other regions for the coarse-scale problem is computed by using the continuum flow theory with a constant viscosity.

Using the embedding multiscale methods, electroosmotic flow inside two 6.00 nm wide channels has been studied. Comparison of the results with the direct MD simulation results indicated that the methods predict the ion distribution and velocity profile with good accuracy. Finally, we have also studied the electroosmotic flow inside a 30 μm wide channel at various bulk concentrations. Simulation results indicated that the classical continuum theory overestimates the average velocity in the channel significantly at a high-bulk concentration, and the error decreases as the bulk concentration decreases.

ACKNOWLEDGMENT

This research was supported in part by grants from NSF and DARPA. R.Q. is supported by a Graduate Fellowship from the Beckman Institute for Advanced Science and Technology at the University of Illinois at Urbana-Champaign.

REFERENCES

1. Harrison, D.J., Fluri, K., Fan, Z., Effenhauser, C.S., and Manz, A. Micromachining a miniaturized capillary electrophoresis-based chemical analysis system on a chip. *Science* **261**:895–897, 1993.
2. Reyes, D.R., Iossifidis, D., Auroux, P.A., and Manz, A. Micro Total Analysis systems. I. Introduction, theory and technology. *Anal. Chem.* **74**(12):2623–2636, 2002.
3. Kemery, P.J., Steehler, J.K., and Bohn, P.W. Electric field mediated transport in nanometer diameter channels. *Langmuir* **14**:2884–2889, 1998.
4. Kuo, T.C., Sloan, L.A., Sweedler, J.V., and Bohn, P.W. Manipulating molecular transport through nanoporous membranes by control of electrokinetic flow: Effect of surface charge density and Debye length. *Langmuir* **17**:6298–6303, 2001.
5. Kuo, T. C., Cannon Jr., D. M., Chen, Y., Shannon, M. A., Tulock, J. J., Sweedler, J. V., and Bohn, P. W. Gateable nanofluidic interconnects for multilayered microfluidic separation systems. *Anal. Chem.* **75**:1861–1867, 2003.
6. Patankar, N. A., and Hu, H. H. Numerical simulation of electroosmotic flow. *Anal. Chem.* **70**:1870–1881, 1998.
7. Ermakov, S. V., Jacobson, S. C., and Ramsey, J. M. Computer simulations of electrokinetic transport in microfabricated channel structures. *Anal. Chem.* **70**:4494–4504, 1998.

8. Mitchell, M.J., Qiao, R., and Aluru, N.R. Meshless analysis of steady-state electro-osmotic transport. *J. Microelectromechanical Systems* **9**(4):435–449, 2000.
9. Hunter, R.J. *Zeta potential in colloid science: principles and applications*. Academic Press, London, 1981.
10. Lyklema, J., Rovillard, S., and Coninck, J.De. Electrokinetics: The properties of the stagnant layer unraveled. *Langmuir* **14**(20):5659–5663, 1998.
11. Poppe, H., Cifuentes, A., and Kok, W.T. Theoretical description of the influence of external radial fields on the electroosmotic flow in capillary electrophoresis. *Anal. Chem.* **68**:888–893, 1996.
12. Qiao, R., and Aluru, N. R. Ion concentrations and velocity profiles in nanochannel electroosmotic flow. *J. Chem. Phys.* **118**:4692–4701, 2003.
13. Hadjiconstantinou, N. G. Hybrid atomistic-continuum formulations and the moving contact-line problem. *J. Comput. Phys.* **154**:245–265, 1999.
14. Atkas, O., and Aluru, N. R. A combined continuum/DSMC technique for multiscale analysis of microfluidic filters. *J. Comput. Phys.* **178**:342–372, 2002.
15. Delgado-Buscalioni, R., and Coveney, P. V. Continuum-particle hybrid coupling for mass, continuum and energy transfer in unsteady fluid flow. *Phys. Rev. E* **67**:046704, 2003.
16. Berendsen, H.J.C., Grigera, J.R., and Straatsma, T.P. The missing term in effective pair potentials. *J. Phys. Chem.* **91**:6269–6271, 1987.
17. van der Spoel, D., van Maaren, P.J., and Berendsen, H.J.C. A systematic study of water models for molecular simulation: derivation of water models optimized for use with a reaction field. *J. Chem. Phys.* **108**(24):10220–10230, 1998.
18. Cummings, P.T., and Varner, Jr., T.L. Nonequilibrium molecular dynamics calculation of the shear viscosity of liquid water. *J. Chem. Phys.* **89**(10):6391–6398, 1989.
19. Lide, D. R., and Frederikse, H.P. R. *CRC Handbook of Chemistry and Physics, 79th Ed.* CRC Press, Cleveland, 1998.
20. Israelachvili, J. *Intermolecular and surface forces*. Academic Press, New York, 1992.
21. Lindahl, E., Hess, B., and van der Spoel, D. Gromacs 3.0: A package for molecular simulation and trajectory analysis. *J. Mol. Mod.* **7**(8):306–317, 2001.
22. Berendsen, H. J. C., van der Spoel, D., and van Drunen, R. Gromacs: A message-passing parallel molecular dynamics implementation. *Comp. Phys. Comm.* **91**:43–56, 1995.
23. Darden, T., York, D., and Pedersen, L. Particle mesh Ewald: an N-logN method for ewald sums in large systems. *J. Chem. Phys.* **98**:10089–10092, 1993.
24. Yeh, I., and Berkowitz, M. Ewald summation for systems with slab geometry. *J. Chem. Phys.* **111**(7):3155–3162, 1999.
25. Allen, M.P., and Tildesley, D.J. *Computer simulations of liquids*. Oxford University Press, New York, 1987.
26. Berendsen, H. J. C., Postma, J. P. M., van Gunsteren, W. F., DiNola, A., and Haak, J. R. Molecular dynamics with coupling to an external bath. *J. Chem. Phys.* **81**:3684–3690, 1984.
27. Freund, J. Electro-osmosis in a nanometer-scale channel studied by atomistic simulation. *J. Chem. Phys.* **116**(5):2194–2200, 2002.